First–in–Class Humanized FSH Blocking Antibody Targets Bone and Fat

[1]Sakshi Gera, [1]Damini Sant, [2]Shozeb Haider, [1]Funda Korkmaz, [1]Gregory Jebian, [3]Hao Chen, [2]Helena Perez-Pena, [3]Zhen Cheng, [1]Kejun Ma, [1]Anne MacDonald, [1]Elina Hadelia, [1]Anisa Gumerova, [1]TanChun Kuo, [1]Mehr Mathew, [1]Anthony Williams, [1]Charit Taneja, [4]Honglin Xie, [1]Hirotaka Miyashita, [1]Kseniia Ievleva, [1]Rogerio Batista, [5]Jiahuan He, [1]Vitaly Ryu, [6]Victoria DeMambro, [7]Marcia Meseck, [1]Se-Min Kim, [1]Jameel Iqbal, [1]Maria I. New, [1]Daria Lizneva, [6]Clifford J. Rosen, [5]Aaron J. Hsueh, [1]Tony Yuen, [1]Mone Zaidi

[1]The Mount Sinai Bone Program, Department of Medicine, Icahn School of Medicine at Mount Sinai, New York, NY 10029, USA; [2]Department of Pharmaceutical and Biological Chemistry, University College London School of Pharmacy, London WC1N 1AX, UK; [3]Molecular Imaging Program at Stanford, Bio-X Program, Department of Radiology, Stanford University, Stanford, CA 94305, USA; [4]GenScript Biotech Corporation, Piscataway, NJ 08854, USA; [5]Department of Obstetrics and Gynecology, Stanford University School of Medicine, Stanford, CA 94305, USA; [6]Center for Clinical and Translational Research, Maine Medical Center Research Institute, Scarborough, ME 04074, USA; [7]Tisch Cancer Institute, Icahn School of Medicine at Mount Sinai, New York, NY 10029, USA.

Corresponding author: Mone Zaidi (mone.zaidi@mssm.edu)

Blocking the action of FSH genetically or pharmacologically in mice reduces body fat, lowers serum cholesterol, and increases bone mass making an anti–FSH agent a potential therapeutic for three global epidemics – obesity, osteoporosis and hypercholesterolemia. Here, we report the generation, structure and function of a first–in–class, fully humanized, epitope–specific FSH blocking antibody with a K_D of 7 nM. Protein thermal shift, molecular dynamics and fine mapping of the FSH–FSH receptor interface confirm stable binding of the antibody to two of five receptor–interacting residues of the FSHβ subunit, which is sufficient to block its interaction with the FSH receptor. In doing so, the humanized antibody profoundly inhibited FSH action in cell–based assays – a prelude to further preclinical and clinical testing.

Obesity and osteoporosis affect nearly 650 and 200 million people worldwide[1,2]. Yet the armamentarium for preventing and treating these disorders remains limited, particularly when compared with public health epidemics of a similar magnitude. It has also become increasingly clear that obesity and osteoporosis track together clinically. First, body mass does not protect against bone loss; instead, obesity can be permissive to osteoporosis and a high fracture risk[3,4]. Furthermore, the menopausal transition marks the onset not only of rapid bone loss, but also of visceral obesity and dysregulated energy balance[5-9]. These physiologic aberrations have been attributed traditionally to a decline in serum estrogen, although, during the perimenopause – two to three years prior to the last menstrual period – serum estrogen is within the normal range, while FSH levels rise to compensate for reduced ovarian reserve[10-12]. In our view, therefore, the early skeletal and metabolic derangements cannot conceivably be explained solely by declining estrogen.

The past decade has shown that pituitary hormones can act directly on the skeleton and other tissues, a paradigm–shift that is in stark contrast to previously held views on their sole regulation of endocrine targets[13-24]. We and others have shown that FSH can bypass the ovary to act on G_i–coupled FSH receptors (FSHRs) on osteoclasts to stimulate bone resorption[23,24]. This mechanism, which could underscore the bone loss during early menopause, is testified by the strong correlations between serum FSH, bone turnover and bone mineral density[7-9,14,25,26]. Likewise, activating polymorphisms in the *FSHR* in postmenopausal women are linked to a high bone turnover and reduced bone mass[27]. To us, it therefore made biological and clinical sense to inhibit FSH action during this period to prevent bone loss.

Towards this goal, we generated murine polyclonal and monoclonal antibodies to a 13–amino–acid–long binding epitope of FSHβ[28-31]. The mouse and human FSHβ epitopes differ by just two amino acids – hence, blocking antibodies to the human epitope showed efficacy in mice[28]. The antibodies attenuated the loss of bone after ovariectomy by inhibiting bone

resorption and stimulating bone formation, and, in addition, displayed profound effects on body composition[28,29,31]. Most notably, in a series of contemporaneously reproduced experiments, we (M.Z. and C.J.R) found that FSH blockade reduced body fat, triggered adipocyte beiging, and increased thermogenesis in models of obesity[29]. Our findings have been further confirmed independently by two groups who used a FSHβ–GST fusion protein or tandem repeats of the 13–amino–acid–long FSHβ epitope for studies on bone and fat, respectively[32,33]. Furthermore, and importantly, inhibiting FSH secretion using a GnRH agonist in patients with prostate cancer resulted in low body fat compared with orchiectomy, wherein FSH levels are high[34]. This interventional clinical trial provides definitive evidence for a therapeutic benefit of reducing FSH levels on body fat in people. There is also new evidence that FSH blockade lowers serum cholesterol[35,36].

Thus, both emerging and validated datasets on the anti–obesity, osteoprotective and lipid–lowering actions of FSH blockade in mice and in humans prompted our current attempt to develop and characterize an array of fully humanized FSH–blocking antibodies for future testing in people. Here, we report that our lead first–in–class humanized antibody, Hu6, and two related molecules, Hu26 and Hu28, bind human FSH with a high affinity (K_Ds <10 nM), block the action of FSH on the human FSHR, and inhibit FSH action in functional cell–based assays.

RESULTS

First–in–Class Humanized Anti–FSHβ Antibodies

Two murine monoclonal anti–FSHβ antibodies, Mf4 and Hf2, developed by us against corresponding mouse and human receptor–binding epitope of the ligand FSHβ, namely LVYKDPARPNTQK and LVYKDPARPKIQK, were validated for biological efficacy in enhancing bone mass in ovariectomized mice[28], and in the case of Hf2, in reducing body fat and inducing adipocyte beiging[29]. When tested for their ability to inhibit osteoclast formation in a cell–based

assay, the antibodies displayed IC_{50}s of 5.4 and 6.1 nM, respectively[28]. Hf2 was selected for humanization and further testing.

The variable domains of the heavy and light IgG chains, V_H and V_L, were amplified from Hf2 hybridomas. A mouse–human chimeric antibody (CH1) was first constructed by cloning the corresponding V_H and V_L together with human IgG_1-C_H and IgK-C_L fragments, respectively, into pTT5 vector. To generate fully humanized antibodies, a bacterial expression library consisting of the antigen–binding fragments (Fab) was produced with single site mutations introduced in the human framework flanking the complementarity–determining region (CDR), while keeping the CDR itself unaltered. This yielded 30 humanized Fab clones (1–30), which were expressed in *E. coli*. Crude supernatant extracts were initially tested for binding to both mouse and human FSHβ in an ELISA (Extended Data Fig.1), followed by further confirmation of FSH–binding by surface plasma resonance (SPR, Biacore) and rank–ordering by dissociation constants (K_ds) (Extended Table. 1). Three full–length high–affinity humanized IgGs with the lowest K_ds were purified (Extended Data Fig. 2); these are henceforth referred to as Hu6, Hu26 and Hu28.

Highly Specific Binding of Hu6, Hu26 and Hu28 to Human FSH

We utilized three complementary approaches to establish the binding of Hu6, Hu26 and Hu28, as well as CH1 to recombinant mouse and human FSH. SPR yielded binding affinities (K_Ds) of 7.52, 10.5 and 12.8 nM to human FSH for Hu6, Hu26 and Hu28, respectively (Fig. 1a and Table 1). The respective antibodies also bound mouse FSHβ with somewhat higher affinities (Extended Data Fig. 3 and Table 1). Such cross–reactivity was expected as the human epitope to which the antibodies were raised was different by just two amino acids from the mouse sequence (NT→KI)[28] – thus allowing us to use murine cell–based models for efficacy testing of the humanized molecule.

We further tested the specificity of antibody binding to human FSH by ELISA, with the plate coated with equal concentrations of human FSH, human LH or human TSH (100 ng each). Binding was assessed using an HRP–conjugated antibody to human IgG following overnight incubation with increasing concentrations of Hu6, Hu26, Hu28 or CH1. Fig. 1b shows concentration–dependent binding of human FSH to all four antibodies, whereas no binding was detected with LH or TSH, or when control human IgG was used.

We confirmed binding of our lead molecule, Hu6, with a protein thermal shift assay that utilizes a fluorescent reporter to detect hydrophobic domains that are exposed following the unfolding of globular proteins with increasing temperature. In the presence of ligand, protein structure is stabilized requiring a higher temperature for it to unfold. Hu6 was incubated with or without human FSH in the presence of Sypro–Orange (Applied Biosystems) at room temperature for 30 min. Fluorescence was captured sequentially at 0.3^{o}C increments using a StepOne Plus Thermocycler (Applied Biosystems). FSH, a protein composed mainly of β–sheets, expectedly showed no increase in fluorescence upon heating. In contrast, Hu6 showed two peaks: one at ~69^{o}C representing unfolding of the Fc domain, and another at 77^{o}C resulting from unfolding of the Fab region (Fig. 1c). Incubation of Hu6 with human FSH produced a dramatic, ~6^{o}C, right–shift of the Fab peak, but not in the Fc peak. The persistence of the right–shift at 83^{o}C was consistent with a stable high–affinity binding of FSH to the Fab domain (Fig. 1c). Of note, and consistent with the ELISA in Fig. 1b, human LH failed to produce a thermal shift (Fig. 1c).

Atom–Level Fine Mapping of Epitope–Antibody Interactions

To study the interaction of Hu6, Hu26, Hu28 and CH1 clones with human and mouse FSHβ in atomistic detail, we modeled the respective variable regions of each antibody clone using Modeller 9.1[37]. The antibody–FSHβ interacting interface was then studied by

HADDOCK[38,39]. To identify interactions that stabilized docked antibody–FSHβ complexes, each complex was subjected to molecular dynamics simulations. RMSD–based clustering identified three clusters, from which the medoid was selected to calculate electrostatic energy (using APBS). Of note is that, while the CDR regions of Hu6, Hu26 and H2u8 are identical, mutations in the flanking region of the CDRs created during humanization caused subtle differences in the FSHβ residues that were recognized by the antibodies (below).

Both V_H and V_L regions of the antibody clones interacted with the targeted epitope residues of human and mouse FSHβ (Fig. 2), with predicted electrostatic energies ($\Delta\Delta$Gs) consistent with K_Ds calculated from the SPR dataset (Table 1). Both human and mouse FSHβ epitopes and V_L region of CH1 displayed the most electrostatic interactions (Fig. 2, Table 2). However, whereas there were no direct interactions between K46 of human FSHβ and CH1, with mouse FSHβ, residue N46 interacted with R44 that then interacted with D104 and Y105 of the V_H region. This latter pattern of atomistic interactions between antibody and residue K/N46 broadly resembled that of Hu6 (Fig. 2 and Table 2). With clone Hu26, in the human complex, K46 made direct hydrogen bonds with D28, S30 and H92 of the V_L region (Fig. 2 and Table 2). In the mouse complex, whereas residue N46 did not directly interact with V_L, it interacted with the guanidinium side chain of R44, which, in turn, interacted with S30, Y32 and H92. Clone Hu28 displayed lesser affinity and reduced interactions with both human and mouse FSHβ (Fig. 2 and Tables 1 and 2). The side chain of residue N46 of mouse FSHβ (and not K46 of human FSHβ) interacted directly with residue Y32 of the V_L region. Displaying the least $\Delta\Delta$G (Table 1), Hu23 interacted minimally with mouse and human FSHβ (Fig. 2 and Table 2). Specifically, residue K/N46 of Hu23 did not interact with the V_L region. However, the R44 side chain of the mouse complex formed a hydrogen bond with Y32, and the carbonyl oxygen of the backbone of P42 interacted with R53 of V_L.

It is interesting that while the humanized molecules were developed using the parent antibody, Hf2, designed against the human FSHβ epitope[28], all clones showed favorable affinities towards mouse FSHβ, which was different in just two amino acids (NT→KI) (Table 1). One explanation is that, with mouse FSHβ, the smaller size of N46 permits direct interactions with the V_L chain of the antibodies; if not, it forms hydrogen bonds with the guanidinium side chain of R44. This internal electrostatic interaction within mouse FSHβ stabilizes the loop structure of its epitope, thus allowing more favorable interactions. In contrast, in the case of human FSHβ, the relatively longer K46 side chain is unable to make internal interactions resulting in charge repulsion with R44. This leads to destabilization of the loop structure causing fewer interactions between the human FSHβ chain and the respective antibodies. Thus, the structure adopted by the epitope sequence and its side chain determines the ability to make inter– and intra–electrostatic interactions.

Hu6, H26 and Hu28 Block FSH–FSHR Interactions

Having fine–mapped the binding interface of the humanized antibodies to FSH, we tested experimentally whether the antibodies blocked the interaction of FSH with its receptor. For this, we created a stable FSHR–overexpressing HEK293 cell line, wherein FSHR was detected by flow cytometry using Alexa647–labeled human FSH (*FSH) or an anti–FSHR antibody (1 in 1000, Invitrogen, #PA-50963) (Fig. 3). Hu6, Hu26 and Hu28, and the chimera, CH1, all prevented *FSH binding to FSHR–overexpressing HEK293 cells in three separate experiments (Fig. 3). Namely, there was a right–shift in fluorescence intensity with *FSH, and this shift was reversed with all FSH blocking antibodies, including our polyclonal antibody (positive control), but not with human IgG (Fig. 3). Of note is that the relatively high concentration (100 nM) of *FSH required for eliciting a fluorescence signal might result from a reduced affinity arising from the labeling of Lys residues (K40, K46, and K49) within the binding

site. This also meant that a higher antibody concentration (10 μM) was required to block binding. The data nonetheless establish that our antibodies effectively block FSH action on the FSHR.

Lead Antibody Hu6 Inhibits FSH Action in Cell–Based Assays

Given our future interest in utilizing humanized anti–FSH antibodies for the treatment of osteoporosis and obesity, we used two cell–based assays to study the FSH blocking action of our lead molecule, Hu6, as well as Hu26 and Hu28. For the first assay, designed to study osteoclast formation, bone marrow hematopoietic cells were incubated with RANKL (50 ng/mL) and MCSF (20 ng/mL) for 5 days with or without FSH (50 ng/mL) and increasing antibody concentrations. As FBS–containing medium was used, we expected that each antibody, by blocking the action of endogenous FSH (up to 78 ng/mL[40]), would reduce osteoclast numbers, quantitated as ACP5–positive cells, in the absence of added FSH – this was indeed the case (Fig. 4a and 4b). The IC_{50}s of the three antibodies were in the sub–nanomolar range (Fig. 4a).

To establish FSH specificity, we first spiked the medium with 50 ng/mL FSH and found that the stimulation by FSH of osteoclastogenesis was attenuated with increasing antibody concentrations (Figs. 4a and 4b). Second, we utilized bone marrow cell cultures from *Fshr*$^{-/-}$ mice, which displayed a reduced propensity to form osteoclasts; the latter finding confirmed an inhibitory effect of FSHR deletion *per se* on osteoclastogenesis (Fig. 4c). More importantly, however, while all three antibodies suppressed osteoclast formation in wild type cultures, compared with IgG, they failed to further suppress osteoclastogenesis in *Fshr*$^{-/-}$ cultures (Fig. 4c). Together, the findings prove that Hu6, Hu26 and Hu28 inhibit osteoclast formation by blocking FSH signaling, a prelude for their testing for osteoprotection in people.

In a second assay, we explored the effects of Hu6 on expression of adipocyte beiging genes in 3T3.L1 cells. Cells were differentiated in the presence of FBS (10%, v/v), rosiglitazone (0.5 μM), dexamethasone (0.25 μM), IBMX (0.125 mM) and insulin (2.5 μg/mL). FSH caused a significant reduction in the expression of *Cox8b*, *Ucp1* and *Prdm16*, but not *Cebpa* (Fig. 4d). Importantly, whereas Hu6 (6.6 nM) itself had no significant effect on gene expression, it reversed the inhibition noted at both FSH concentrations (10 and 30 ng/mL) (Fig. 4d). This effect, consistent with our proof–of–concept polyclonal antibody data[29], provides the framework for studying the pro–beiging and thermogenic efficacy of Hu6 in *in vivo* models.

Indeed, we have shown previously, using real time PCR and/or Sanger sequencing, that *Fshrs* are expressed in 3T3.L1 cells, primary adipocytes and mouse adipose tissue[29]. For direct confirmation that FSH binds these receptors, we (A.H.) utilized FSH-CH, a synthetic conjugate of human FSH and CH1055; the latter is a near-infrared II (NIR-II) fluorophore. Incubation of 3T3-L1 cells with FSH-CH resulted in a concentration–dependent increase in the NIR-II signal, which was attenuated strongly upon addition of a 100–fold molar access, i.e. 42 μg/mL, of non–conjugated FSH (K_D – 3.7 nM) (Fig. 4e). We further confirmed binding to fat tissue in Balb/c mice injected with FSH-CH with or without 30X unconjugated FSH. NIR-II signals were detected in the ovaries, skeleton, liver and white and brown adipose tissue; these signals were attenuated in the presence of excess unconjugated FSH, confirming specificity (Extended Data Fig. 4).

DISCUSSION

Here we report the development of, and a full compendium of structural and functional studies on, a first–in–class humanized FSH–blocking antibody targeted to a 13–amino–acid–long receptor–binding epitope of the FSHβ subunit. We have shown previously that targeting this sequence blocks the binding of FSHβ to the FSHR, and in doing so, inhibits bone

resorption, promotes bone formation, increases bone mass, reduces body fat and enhances thermogenesis in mice[29,30,41]. Recent contemporaneous studies using a GST– FSHβ fusion protein or tandem repeats of the epitope provide confirmatory evidence for osteoprotection and weight loss[32,33]. Given the mounting evidence across species for direct actions of FSH on bone[24,28,29,31,33], adipose tissue[29,32,42,43] and liver[35,36], we sought to create a single FSH–blocking agent to treat three global epidemics that affect millions of women and men – namely obesity, osteoporosis and hyperlipidemia. We therefore humanized our murine monoclonal antibody, Hf2, which was raised against a corresponding human FSHβ sequence[28] – this generated 30 clones, from which we selected our lead molecule, Hu6, with the highest affinity and lowest dissociation constant.

We chose not to target full–length FSHβ; instead, we fine–mapped the receptor binding sequence from the available human co–crystal (PDB id 4AY9) and our computational model of the mouse complex[28,30,41]. With largely similar binding modes, we mapped V38, Y39, A43, R44 and K49 as the only receptor–interacting residues in the human FSHβ sequence, with an additional interaction of residue D41 in the mouse[28]. Here, we find that Hu6 binds two of these interacting residues, Y39 and A43, whereas Hu28 binds R44 and K49. In contrast, Hu26 and Hu23 bind only a single interacting residue. Thus, by purposefully creating atom–level maps between FSH and FSHR[28] and between FSH and the antibodies, we were able to confirm Hu6, which bound two centrally–positioned residues, as our lead molecule. Its affinity of ~7 nM is close to that of the HER2 blocker trastuzumab (K_D ~5 nM)[44]. A higher affinity might not be required, as *Fshr* haploinsufficiency phenocopies the effect of blocking FSH with our antibodies[29].

We further utilized complementary methods, namely ELISA, SPR and importantly, the protein thermal shift assay, to document unequivocally the binding of Hu6 (and other humanized versions) to human FSH. Likewise, we show that Hu6 blocks FSH from binding to the FSHR,

and in doing so, inhibits FSH action in functional cell–based assays for osteoclast formation and beiging gene expression. We propose now to take Hu6 as a lead molecule into *in vivo* efficacy and safety testing and clinical development, with the ultimate goal of co–treating osteoporosis, obesity and perhaps hyperlipidemia with a single agent.

Needless to say, the correlation between the onset of bone loss and visceral obesity during the menopausal transition is overwhelmingly strong[5-7,10,11] – this may, at least in principle, warrant an FSH blocking drug to prevent and/or treat both disorders. However, several recent observations reaffirm the rationale for its use not only in menopausal women, but also in men. First, as in mice[24,28,29,31-33], suppressing serum FSH in a controlled setting in humans results in both weight loss and bone gain. A randomized interventional trial showed that prostate cancer patients receiving a GnRH agonist, triptorelin, which drops FSH levels, had lower body weight and body fat compared with those who underwent orchiectomy, where serum FSH levels are invariably high[34]. Selective FSH inhibition could likewise be used as a strategy to protect against bone loss and obesity that accompany low–estrogen states, including surgical or drug–induced menopause, or genetic disorders, such as Turner's syndrome, where persistently elevated FSH levels could be primary drivers. Indeed, in a direct comparison, hypoestrogenemic women with low serum FSH levels lost less bone than those with hypergonadotropic hypogonadism[45]. Finally, there is evidence that reducing serum FSH using a blocking antibody in mice can lower serum cholesterol[35,36], a finding that might, if proven, extend the use of such an agent to control hyperlipidemia.

ACKNOWLEDGEMENTS

M.Z. is grateful to the National Institutes of Health for grant support, namely U19 AG60917 (to M.Z. and C.J.R.) and R01 DK113627 (to M.Z.). M.I.N. is supported by the Maria I. New Children's Hormone Research Foundation.

DISCLOSURES

M.Z. is inventor on patents on FSH, bone and body fat regulation. These patents are owned by Icahn School of Medicine at Mount Sinai, with M.Z. being recipient of royalties should they arise *per* institutional policies. M.Z. also consults for several financial platforms, including Gerson Lehrman Group and Guidepoint, on drugs for osteoporosis and genetic bone diseases.

CONTRIBUTIONS

S.G. was responsible for, performing and overseeing the design, execution and analysis of all experiments; D.S. performed *in vitro* assays, and analyzed and computed certain datasets; S.H. and H.P.-P. carried out fine mapping and molecular dynamics after initial modeling by S.G. and T.K.; M. Mathew and A.G. helped with osteoclast and adipocyte isolation and culture; C.T. and G.J. performed osteoclast counting independently; H.C., Z.C., J.H. and A.J.H. synthesized FSH-CH and performed and analyzed spectroscopic experiments at Stanford; H.X. from GenScript generated the antibodies and carried out initial binding studies (fee–for–service); D.L. helped with FACS analysis; A.W., R.B. and H.M. purified antibodies overseen by S.M.-K.; K.M., A.W. and F.K. raised and maintained mouse colonies; E.H. and K.I. helped with RNA extraction, cDNA preparation and qPCR; V.D., J.I. and C.J.R. independently re-analyzed the entire datasets; A.M., J.I. and M. Meseck wrote and set up procedures for GLP and oversaw data integrity; M.Z., T.Y., V.R., M.I.N. and S.G. designed the experiments and wrote and edited the manuscript.

METHODS

Generation of Humanized FSH Blocking Antibodies: We utilized our murine monoclonal anti–FSHβ antibody Hf2, which was previously generated against the receptor–binding epitope of human FSHβ, namely LVYKDPARPKIQK, and validated functionally for its ability to inhibit osteoclasts, enhance bone mass and reduce body fat[28,29]. Rapid amplification of cDNA ends (RACE) was first used to amplify the variable domains of the heavy and light IgG chains, V_H and V_L, of the Hf2 hybridoma. We then constructed a mouse–human chimeric antibody (CH1) by cloning the V_H and V_L together with human IgG_1-C_H and IgK-C_L fragments into pTT5 vector. CH1 was expressed in HEK293 cells, the supernatants purified with a protein A affinity column, and the purified antibody buffer–exchanged into PBS using a PD-10 desalting column. We then performed homology modeling on the variable domain sequences of CH1 to determine framework residues in the inner core, following which, one human acceptor for V_H and V_L that shared the highest sequence homology to the mouse counterparts was selected. CDRs of CH1 were then grafted into the human acceptor framework. Single site saturation mutagenesis using NNK degenerate codons was utilized to generate a library of the antigen–binding fragments (Fabs) with mutations flanking the CDR, which were subcloned into the pFASEBA vector. The resulting 30 humanized Fab clones (1–30) were expressed in *E. coli*, and crude supernatant extracts were tested for binding to both mouse and human FSHβ in an ELISA (Extended Data Fig. 1). This was followed by further confirmation of FSH–binding by SPR (Biacore 8K/T200) and rank–ordering by dissociation constants (K_ds) (Extended Data Table 1). Following sequencing, cDNAs encoding three high–affinity humanized IgGs with the lowest K_ds, namely, clones 6, 26 and 28, were subcloned into pTT5 vector for expression in HEK293 cells, and the resulting IgGs were purified by protein A affinity chromatography. Biacore was used to measure kinetics and binding affinity of the three purified candidates, namely Hu6, Hu26 and Hu28, and CH1 with human and mouse FSH (Extended Data Fig. 2).

Protein Thermal Shift Assay: The thermal shift assay used a fluorescent reporter, Sypro–Orange (Applied Biosystems), to detect hydrophobic domains that are exposed following the heat–induced unfolding of globular proteins. Hu6 (1.5 μg/μL) was incubated with or without human FSH or human LH (both at 0.5 μg/μL) at room temperature for 30 min, with fluorescence captured sequentially at 0.3^{o}C increments using a StepOne Plus Thermocycler (Applied Biosystems). Tm was calculated based on the inflection point of the melt curve, and the thermal shift was derived from $\Delta Tm = Tm_{Ab+FSH(or\ LH)} - Tm_{Ab}$.

Molecular Dynamics Simulations and Fine Mapping of Antibody–FSH Interface: The crystal structure of human FSH in complex with the entire ectodomain of human FSHR (PDB id 4AY9) was used as a template to model mouse FSH, as before[28,29]. The sequence of mouse FSH was obtained from UniProt (α chain: id P01215; β chain: id Q60687). Using a human IgG template (PDB id: 1FGV and 3AUV), we constructed homology models of the variable regions of the humanized antibodies, Hu6, Hu26, Hu28 and Hu23, and the chimera CH1, using Modeller [46]. We confirmed stereochemical parameters using PROCHECK and PROSA[47]. The interacting interface between FSHβ and each modeled structure was examined by HADDOCK[38,39], and clusters with the lowest Root Means Squared Deviation (RMSD) were selected for fine mapping. For molecular dynamics simulations, models of the docked complexes were prepared using Protein-Prepare implemented in the HTMD suite[48]. 13 disulphide bonds were introduced into the FSHα and FSHβ chains, and the complex parameterized using Amberff14SB force field and solvated in a TIP3P waterbox, with edges extending ≥10 Å from the solute. For each model, 5 ns of NPT ensemble was run to equilibrate the system, followed by a production run of 250 ns in NVE ensemble using Acemd MD engine (www.acellera.com). The timestep was kept at 4 fs; periodic boundary conditions were utilized; and the accuracy of the particle mesh Ewald was increased, while direct sum tolerance was reduced by an order of magnitude (0.000001).

RMSD–based clustering was carried out using Biki Life Sciences Suite[49]. For calculating electrostatic binding energy (ΔΔG), the medoid from the largest of the three clusters was used. Ionization states (pKa) of the side chains were identified using PROPKA[50] as implemented on the PDB2PQR server[51]. Adaptive Poisson Boltzmann equation was solved to calculate the electrostatic interactions between FSH and antibodies using APBS[52]. Figures were generated using MolSoft ICM-Pro Suite (www.molsoft.com) and ezCADD[53].

Flow Cytometry: We created a stable FSHR–overexpressing HEK293 cell line. FSHR protein expression was detected with Alexa647–labelled human FSH (*FSH) (100 nM) or an anti–FSHR antibody (1 in 1000, Invitrogen, #PA-50963) by flow cytometry (CytoFLEX, Beckman Coulter). *FSH was added with or without Hu6, Hu26, Hu28, or CH1 (all at 10 μM). Untransfected cells were used as specificity controls – there were no shifts with FSHR Ab, secondary antibody, or *FSH. Median fluorescence intensity (MFI) was determined from three separate experiments.

Cell Based Assays: To study osteoclast formation, bone marrow hematopoietic cells from wild type mice, or to establish FSH–specificity, from *Fshr*$^{-/-}$ mice, were incubated with RANKL (50 ng/mL) and MCSF (20 ng/mL) for 5 days with or without FSH (50 ng/mL) and antibodies Hu6, Hu26 or Hu28, or human IgG (negative control). Osteoclast numbers were quantitated blindly as cells positive for tartrate–resistant acid phosphatase type 5 (ACP5) using a kit (Sigma; #386A-1KT). IC_{50}s of the three antibodies were calculated using GraphPad Prism. To study the effects of Hu6 on the expression of adipocyte beiging genes, we cultured 3T3-L1 cells in medium containing FBS (10%, v/v), for 3 days in sub–maximal (0.25X) differentiation conditions [rosiglitazone (0.5 μM), dexamethasone (0.25 μM), IBMX (0.125 mM) and insulin (2.5 μg/mL)], and for further 9 days in insulin (2.5 μg/mL) in the presence of Hu6 with or without FSH (10 or 30 ng/mL). *Cox8b*, *Ucp1* and *Prdm16*, *Cebpa* gene expression was studied using quantitative PCR with SYBR Green and validated primer sets, as in Liu *et al.*[29]

REFERENCES

1 International Osteoporosis Foundation. *Osteoporosis - Incidence and burden*, <https://www.iofbonehealth.org/facts-statistics - category-13> (2016).

2 World Health Organization. *Obesity and Overweight*, <https://www.who.int/news-room/fact-sheets/detail/obesity-and-overweight> (2018).

3 Zaidi, M., Buettner, C., Sun, L. & Iqbal, J. Minireview: The link between fat and bone: does mass beget mass? *Endocrinology* **153**, 2070-2075, doi:10.1210/en.2012-1022 (2012).

4 Greco, E. A. *et al.* Is obesity protective for osteoporosis? Evaluation of bone mineral density in individuals with high body mass index. *Int J Clin Pract* **64**, 817-820, doi:10.1111/j.1742-1241.2009.02301.x (2010).

5 Sowers, M., Pope, S., Welch, G., Sternfeld, B. & Albrecht, G. The association of menopause and physical functioning in women at midlife. *Journal of the American Geriatrics Society* **49**, 1485-1492 (2001).

6 Sowers, M. *et al.* Changes in body composition in women over six years at midlife: ovarian and chronological aging. *J Clin Endocrinol Metab* **92**, 895-901, doi:10.1210/jc.2006-1393 (2007).

7 Sowers, M. R. *et al.* Hormone predictors of bone mineral density changes during the menopausal transition. *J Clin Endocrinol Metab* **91**, 1261-1267, doi:10.1210/jc.2005-1836 (2006).

8 Sowers, M. R. *et al.* The association of endogenous hormone concentrations and bone mineral density measures in pre- and perimenopausal women of four ethnic groups: SWAN. *Osteoporos Int* **14**, 44-52, doi:10.1007/s00198-002-1307-x (2003).

9 Sowers, M. R. *et al.* Endogenous hormones and bone turnover markers in pre- and perimenopausal women: SWAN. *Osteoporos Int* **14**, 191-197, doi:10.1007/s00198-002-1329-4 (2003).

10 Randolph, J. F., Jr. *et al.* Change in estradiol and follicle-stimulating hormone across the early menopausal transition: effects of ethnicity and age. *J Clin Endocrinol Metab* **89**, 1555-1561, doi:10.1210/jc.2003-031183 (2004).

11 Randolph, J. F., Jr. *et al.* Change in follicle-stimulating hormone and estradiol across the menopausal transition: effect of age at the final menstrual period. *J Clin Endocrinol Metab* **96**, 746-754, doi:10.1210/jc.2010-1746 (2011).

12 Randolph, J. F., Jr. *et al.* Reproductive hormones in the early menopausal transition: relationship to ethnicity, body size, and menopausal status. *J Clin Endocrinol Metab* **88**, 1516-1522, doi:10.1210/jc.2002-020777 (2003).

13 Abe, E. *et al.* TSH is a negative regulator of skeletal remodeling. *Cell* **115**, 151-162, doi:10.1016/s0092-8674(03)00771-2 (2003).

14 Cannon, J. G. *et al.* Follicle-stimulating hormone, interleukin-1, and bone density in adult women. *American Journal of Physiology-Regulatory, Integrative and Comparative Physiology* **298**, R790-R798 (2009).

15 Stilley, J. A. *et al.* FSH receptor (FSHR) expression in human extragonadal reproductive tissues and the developing placenta, and the impact of its deletion on pregnancy in mice. *Biology of reproduction* **91**, 74, 71-15 (2014).

16 Sun, L. *et al.* Oxytocin regulates body composition. *Proc Natl Acad Sci U S A*, doi:10.1073/pnas.1913611116 (2019).

17 Sun, L. *et al.* FSH directly regulates bone mass. *Cell* **125**, 247-260, doi:10.1016/j.cell.2006.01.051 (2006).

18 Sun, L. *et al.* Functions of vasopressin and oxytocin in bone mass regulation. *Proc Natl Acad Sci U S A* **113**, 164-169, doi:10.1073/pnas.1523762113 (2016).

19 Tamma, R. *et al.* Oxytocin is an anabolic bone hormone. *Proc Natl Acad Sci U S A* **106**, 7149-7154, doi:10.1073/pnas.0901890106 (2009).
20 Wang, J. *et al.* Follicle-Stimulating Hormone Increases the Risk of Postmenopausal Osteoporosis by Stimulating Osteoclast Differentiation. *PLoS One* **10**, e0134986, doi:10.1371/journal.pone.0134986 (2015).
21 Zaidi, M. Skeletal remodeling in health and disease. *Nat Med* **13**, 791-801, doi:10.1038/nm1593 (2007).
22 Zaidi, M. *et al.* Actions of pituitary hormones beyond traditional targets. *J Endocrinol* **237**, R83-R98, doi:10.1530/JOE-17-0680 (2018).
23 Robinson, L. J. *et al.* FSH-receptor isoforms and FSH-dependent gene transcription in human monocytes and osteoclasts. *Biochem Biophys Res Commun* **394**, 12-17, doi:10.1016/j.bbrc.2010.02.112 (2010).
24 Sun, L. *et al.* FSH directly regulates bone mass. *Cell* **125**, 247-260 (2006).
25 Zaidi, M. *et al.* FSH, Bone Mass, Body Fat, and Biological Aging. *Endocrinology* **159**, 3503-3514, doi:10.1210/en.2018-00601 (2018).
26 Cheung, E. *et al.* Bone loss during menopausal transition among southern Chinese women. *Maturitas* **69**, 50-56, doi:10.1016/j.maturitas.2011.01.010 (2011).
27 Rendina, D. *et al.* FSHR gene polymorphisms influence bone mineral density and bone turnover in postmenopausal women. *European journal of endocrinology* **163**, 165-172 (2010).
28 Ji, Y. *et al.* Epitope-specific monoclonal antibodies to FSHbeta increase bone mass. *Proc Natl Acad Sci U S A* **115**, 2192-2197, doi:10.1073/pnas.1718144115 (2018).
29 Liu, P. *et al.* Blocking FSH induces thermogenic adipose tissue and reduces body fat. *Nature* **546**, 107 (2017).
30 Zhu, L. L. *et al.* Blocking FSH action attenuates osteoclastogenesis. *Biochem Biophys Res Commun* **422**, 54-58, doi:10.1016/j.bbrc.2012.04.104 (2012).
31 Zhu, L.-L. *et al.* Blocking antibody to the β-subunit of FSH prevents bone loss by inhibiting bone resorption and stimulating bone synthesis. *Proceedings of the National Academy of Sciences* **109**, 14574-14579 (2012).
32 Han, X. *et al.* A novel follicle-stimulating hormone vaccine for controlling fat accumulation. *Theriogenology* **148**, 103-111, doi:10.1016/j.theriogenology.2020.03.005 (2020).
33 Geng, W. *et al.* Immunization with FSHbeta fusion protein antigen prevents bone loss in a rat ovariectomy-induced osteoporosis model. *Biochem Biophys Res Commun* **434**, 280-286, doi:10.1016/j.bbrc.2013.02.116 (2013).
34 Østergren, P. B. *et al.* Luteinizing hormone-releasing hormone agonists are superior to subcapsular Orchiectomy in lowering testosterone levels of men with prostate cancer: results from a randomized clinical trial. *The Journal of urology* **197**, 1441-1447 (2017).
35 Guo, Y. *et al.* Blocking FSH inhibits hepatic cholesterol biosynthesis and reduces serum cholesterol. *Cell Res* **29**, 151-166, doi:10.1038/s41422-018-0123-6 (2019).
36 Song, Y. *et al.* Follicle-stimulating hormone induces postmenopausal dyslipidemia through inhibiting hepatic cholesterol metabolism. *The Journal of Clinical Endocrinology* **101**, 254-263 (2016).
37 Webb, B. & Sali, A. Comparative protein structure modeling using MODELLER. *Current protocols in bioinformatics* **54**, 5.6. 1-5.6. 37 (2016).
38 Van Zundert, G. *et al.* The HADDOCK2. 2 web server: user-friendly integrative modeling of biomolecular complexes. *Journal of molecular biology* **428**, 720-725 (2016).
39 Wassenaar, T. A. *et al.* WeNMR: structural biology on the grid. *Journal of Grid Computing* **10**, 743-767 (2012).

40 Akbar, A. M., Reichert, L. E., Jr., Dunn, T. G., Kaltenbach, C. C. & Niswender, G. D. Serum levels of follicle-stimulating hormone during the bovine estrous cycle. *J Anim Sci* **39**, 360-365, doi:10.2527/jas1974.392360x (1974).
41 Zhu, L. L. *et al.* Blocking antibody to the beta-subunit of FSH prevents bone loss by inhibiting bone resorption and stimulating bone synthesis. *Proc Natl Acad Sci U S A* **109**, 14574-14579, doi:10.1073/pnas.1212806109 (2012).
42 Cui, H. *et al.* FSH stimulates lipid biosynthesis in chicken adipose tissue by upregulating the expression of its receptor FSHR. *J Lipid Res* **53**, 909-917, doi:10.1194/jlr.M025403 (2012).
43 Liu, X. M. *et al.* FSH regulates fat accumulation and redistribution in aging through the Galphai/Ca(2+)/CREB pathway. *Aging Cell* **14**, 409-420, doi:10.1111/acel.12331 (2015).
44 Genentech. in *Herceptin (Package Insert)* (ed Food and Drug Administration) (1998).
45 Devleta, B., Adem, B. & Senada, S. Hypergonadotropic amenorrhea and bone density: new approach to an old problem. *J Bone Miner Metab* **22**, 360-364, doi:10.1007/s00774-004-0495-1 (2004).
46 Fiser, A. & Sali, A. Modeller: generation and refinement of homology-based protein structure models. *Methods Enzymol* **374**, 461-491, doi:10.1016/S0076-6879(03)74020-8 (2003).
47 Wiederstein, M. & Sippl, M. J. ProSA-web: interactive web service for the recognition of errors in three-dimensional structures of proteins. *Nucleic Acids Res* **35**, W407-410, doi:10.1093/nar/gkm290 (2007).
48 Doerr, S., Harvey, M. J., Noe, F. & De Fabritiis, G. HTMD: High-Throughput Molecular Dynamics for Molecular Discovery. *J Chem Theory Comput* **12**, 1845-1852, doi:10.1021/acs.jctc.6b00049 (2016).
49 Decherchi, S., Bottegoni, G., Spitaleri, A., Rocchia, W. & Cavalli, A. BiKi Life Sciences: A New Suite for Molecular Dynamics and Related Methods in Drug Discovery. *J Chem Inf Model* **58**, 219-224, doi:10.1021/acs.jcim.7b00680 (2018).
50 Olsson, M. H., Sondergaard, C. R., Rostkowski, M. & Jensen, J. H. PROPKA3: Consistent Treatment of Internal and Surface Residues in Empirical pKa Predictions. *J Chem Theory Comput* **7**, 525-537, doi:10.1021/ct100578z (2011).
51 Dolinsky, T. J., Nielsen, J. E., McCammon, J. A. & Baker, N. A. PDB2PQR: an automated pipeline for the setup of Poisson-Boltzmann electrostatics calculations. *Nucleic Acids Res* **32**, W665-667, doi:10.1093/nar/gkh381 (2004).
52 Jurrus, E. *et al.* Improvements to the APBS biomolecular solvation software suite. *Protein Sci* **27**, 112-128, doi:10.1002/pro.3280 (2018).
53 Tao, A. *et al.* ezCADD: A Rapid 2D/3D Visualization-Enabled Web Modeling Environment for Democratizing Computer-Aided Drug Design. *J Chem Inf Model* **59**, 18-24, doi:10.1021/acs.jcim.8b00633 (2019).

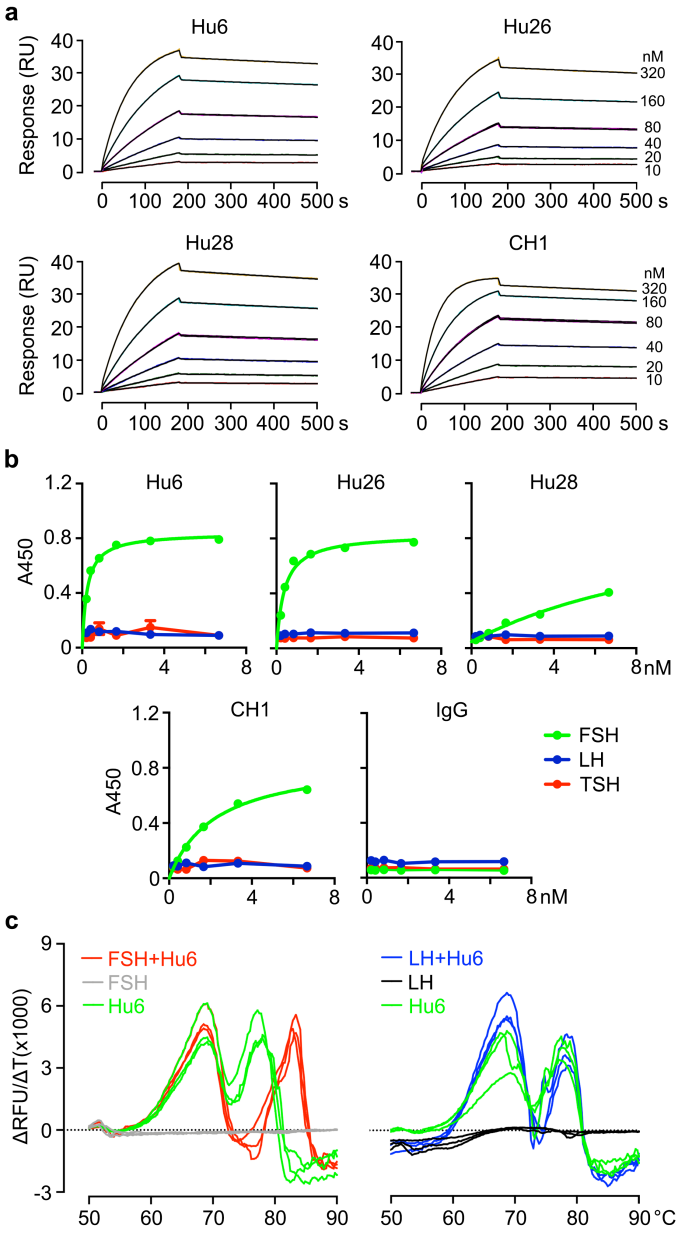

Figure 1: Humanized anti–FSHβ Antibodies Specifically Bind Human FSH. (**a**) Sensograms from surface plasmon resonance measurements (Biacore 8K/T200) showing the concentration–dependent binding of humanized antibodies Hu6, Hu26 and Hu28 (10 – 320 nM) to human FSH. Please also refer to Table 1. (**b**) ELISA showing binding of Hu6, Hu26, Hu28 or CH1 to human FSH (green), but not to human LH (blue) or human TSH (red) (100 ng each) detected with HRP–conjugated antibody to human IgG. No binding with human IgG. Mean of duplicate wells. (**c**) Protein thermal shift assay utilizes Sypro Orange to capture hydrophobic domains during heat–induced protein unfolding to yield a melting temperature, Tm. Change in fluorescence is shown as relative fluorescence units (ΔRFU) per unit change in temperature (ΔT). Hu6 (green traces) showed two peaks: one at ~69^{o}C, caused by the unfolding of the Fc domain, and the other at 77^{o}C, due to unfolding of Fab region. The addition of human FSH (red traces), but not human LH (blue traces), produced a ~6^{o}C thermal shift solely in the Fab peak, indicating binding of FSH to the Fab domain of Hu6. FSH (grey traces) and LH (black traces), which are composed mainly of β–sheets, showed no unfolding.

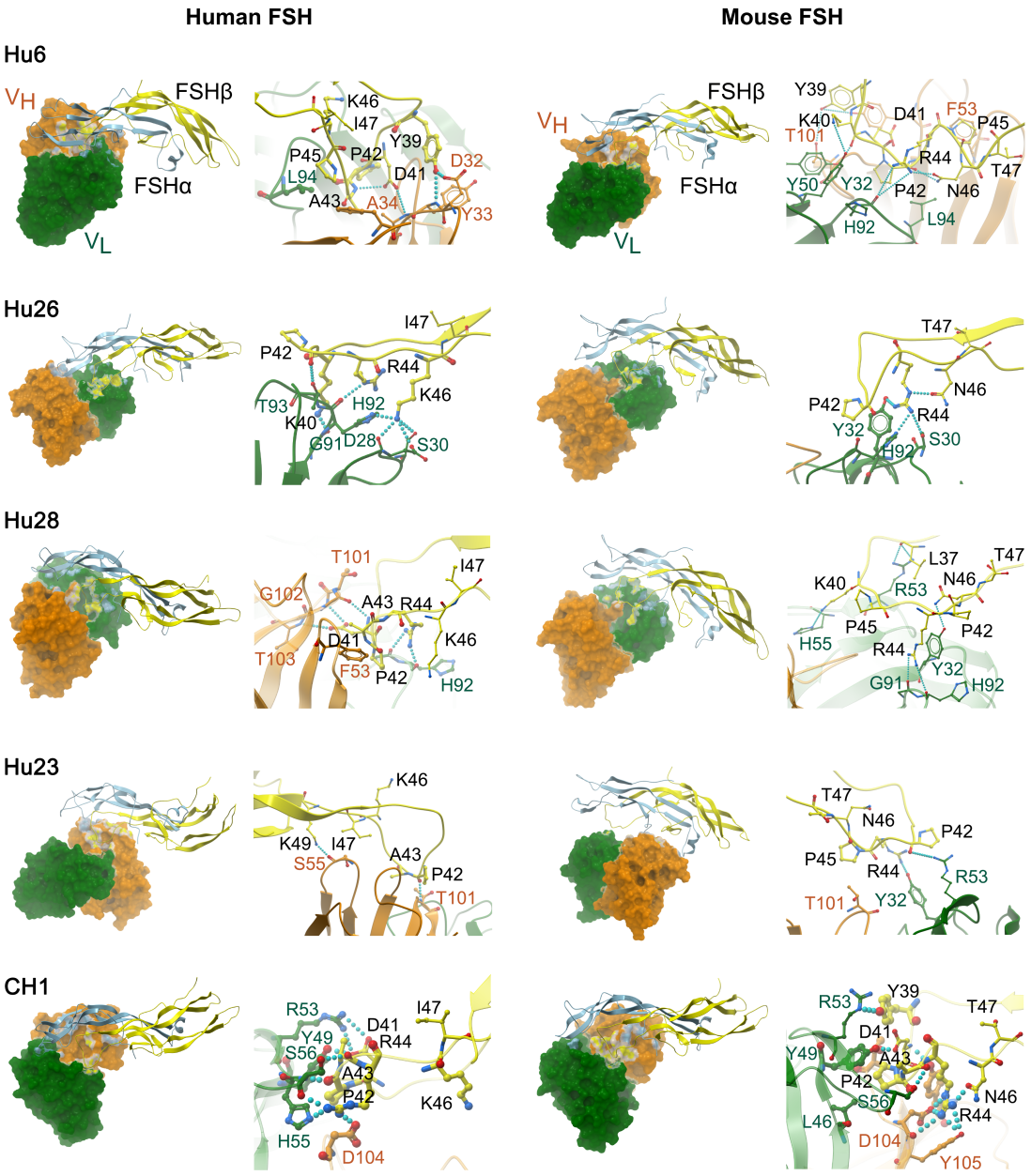

Figure 2: Atom–Level Fine Mapping of Antibody–FSH Interfaces. Shown are computational models and fine maps of complexes between the α (blue) and β (yellow) subunits of FSH, and the variable regions, V_L (green) and V_H (orange), of the humanized monoclonal antibodies Hu6, Hu26, Hu28 and Hu23, as well as the mouse-human chimeric antibody CH1. Interactions between specific amino acids are shown (Please also refer to Table 2).

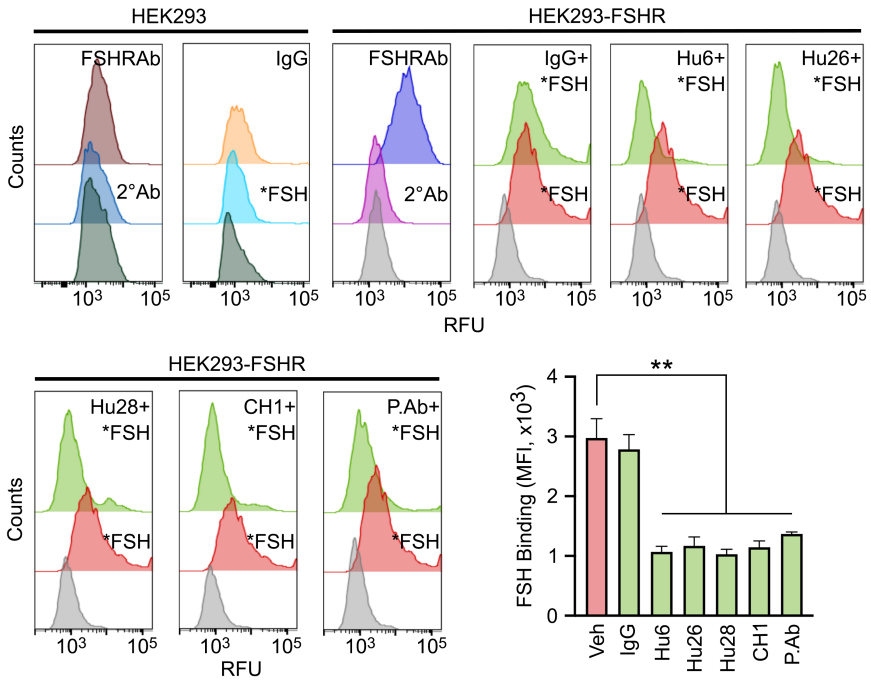

Figure 3: Humanized Antibodies Block FSH Binding to the FSH Receptor.
Representative flow cytometry histograms showing binding of Alexa647–FSH (*FSH) (red) to HEK293 cells that were stably transfected to express human FSHR [confirmed by FSHR antibody (Ab) (Invitrogen #PA-50963), shown in purple]. Of note is that the FSH blocking antibodies Hu6, Hu26 and H28, the mouse-human chimera CH1, and the epitope–targeted polyclonal antibody inhibited *FSH binding (light green). Grey histograms – no added *FSH. Expectedly, no shifts with FSHR Ab, secondary (2^O) Ab, or *FSH in untransfected HEK293 cells. Inhibition of *FSH binding shown as median fluorescence intensity (MFI). Mean ± SEM from three experiments; unpaired Student's t-test; **P<0.01. Relative fluorescence unit (RFU).

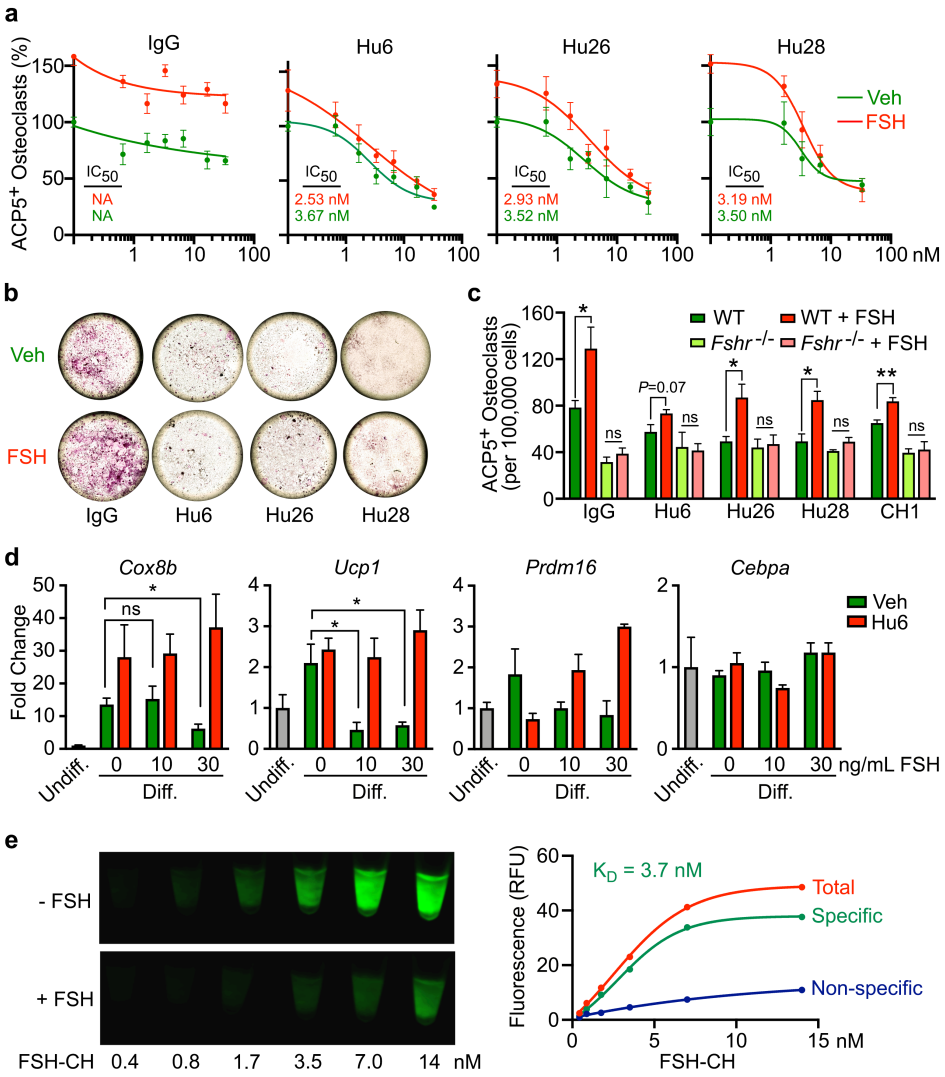

Figure 4: Functional Inhibition by Humanized Antibodies of FSH Action in Cell–Based Assays. Full concentration–response curves (**a**), and representative light micrographs for the highest antibody concentration (66 nM) (**b**) displaying the inhibition of ACP5–positive osteoclast formation in bone marrow cell cultures (50 ng/mL RANKL and 20 ng/mL MCSF) in response to Hu6, Hu26 or Hu28 with or without human FSH (50 ng/mL). Calculated IC_{50}s are shown. (**c**) Inhibition by Hu6, Hu26 and Hu28 (6.6 nM) of FSH–induced osteoclastogenesis in wild type mice (with intact FSHRs) was not seen in cultures from $Fshr^{-/-}$ mice, proving that the antibodies act via the FSH axis. (**d**) Expression of beiging genes, namely *Cox8b*, *Ucp1*, *Prdm16* and *Cebpa* in response to Hu6 (6.6 nM) and/or FSH (10 or 30 ng/ml) in 3T3-L1 cell cultures under differentiating conditions (see 'Methods'). (**e**) 3T3-L1 cells grown in differentiation medium with 10 μM troglitazone for 8 days were incubated with FSH-CH for 2 hours (37^{o}C) with or without a 100–fold molar excess (1.4 μM) of unconjugated FSH. Cells were scanned using Li-Cor Scanner (800 nm channel). Scanned images (left panel) and saturation curves based on quantitation of scanned images (right panel) are shown (KD – 3.7 nM). Mean ± SEM; N = 6, 4 and 3 for panels a, c and d, respectively. Statistics: Unpaired two-tailed Student's t-test, *P<0.05, **P<0.01, or as shown. ns - not significant.

Anti-FSHβ Ab	FSH	K_a ($10^3 M^{-1}s^{-1}$)	K_d ($10^{-6}s^{-1}$)	K_D (nM)	ΔΔG (kJ/mol)
Hu6	Human	23.50	176	7.52	-358
	Mouse	44.50	109	2.45	-409
Hu26	Human	16.90	178	10.50	-316
	Mouse	31.70	113	3.56	-293
Hu28	Human	17.90	229	12.80	-306
	Mouse	34.60	107	3.09	-346
Hu23	Human	30.20	2180	72.40	-278
	Mouse	ND	ND	ND	-255
CH1	Human	43.60	175	4.02	-405
	Mouse	74.10	920	1.24	-435

Table 1: Binding Properties of Humanized FSH–Blocking Antibodies. Surface plasmon resonance (SPR, Biacore 8K/T200) was utilized to study the binding properties of human and mouse FSH with the purified humanized antibodies Hu6, Hu26, Hu28, and Hu23, as well as human–mouse chimeric molecule CH1. These yielded measures of association constant (K_a), dissociation constant (K_d) and affinity (K_D). The K_D values were consistent with *in silico* global net electrostatic binding energies (ΔΔG) calculated from molecular dynamics using APBS. Hu6 displayed the highest K_D and lowest K_d and was thus chosen as the lead molecule for development. ND – not determined. Please also refer to Fig. 1a and Extended Data Fig. 3.

Anti-FSHβ Ab	FSH	L 37	V 38	Y 39	K 40	D 41	P 42	A 43	R 44	P 45	K/N 46	I/T 47	Q 48	K 49
Hu6	Human			●		●	●	●						
	Mouse			●	●	●	●	●	●		●			
Hu26	Human				●		●		●		●			
	Mouse	●					●		●		●			
Hu28	Human					●			●					●
	Mouse				●				●		●			
Hu23	Human					●								
	Mouse					●								
CH1	Human					●	●	●	●					
	Mouse			●		●	●	●	●		●			

Table 2: Antibody–Binding Residues of the Targeted FSHβ Epitope. *In silico* fine mapping of residues of the targeted 13–amino–acid–long human or mouse FSHβ epitope that interact with specific residues of the variable chain of the antibodies Hu6, Hu26, Hu28 and Hu23, as well as the mouse-human chimera (CH1). The five residues that are known to interact with the FSHR[28] have been identified by vertical shades. Please read together with Fig. 2.

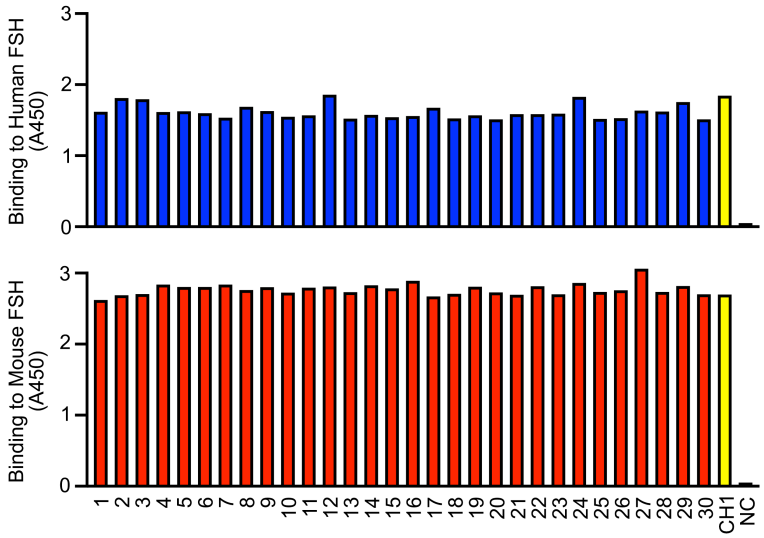

Extended Data Figure 1: Confirmation of Binding of Humanized Antibody Clones to FSH. ELISA using plates coated with human (top panel) or mouse FSH (bottom panel). Binding was measured using HRP–conjugated mouse or human IgG after incubation of bacterial lysates from 30 humanized antibody clones (1-30) and the human–mouse chimera (CH1). NC – negative control without any IgG.

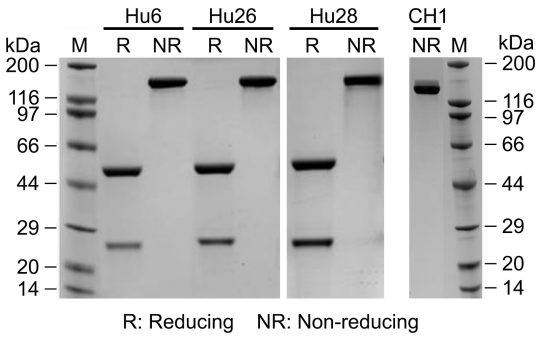

Extended Data Figure 2: Purification of Selected Humanized Antibody Clones. SDS PAGE analysis of Hu6, Hu26, Hu28 and CH1 purified by protein A chromatography. Each IgG (5 μg) was run under reducing (R) and non–reducing (NR) conditions.

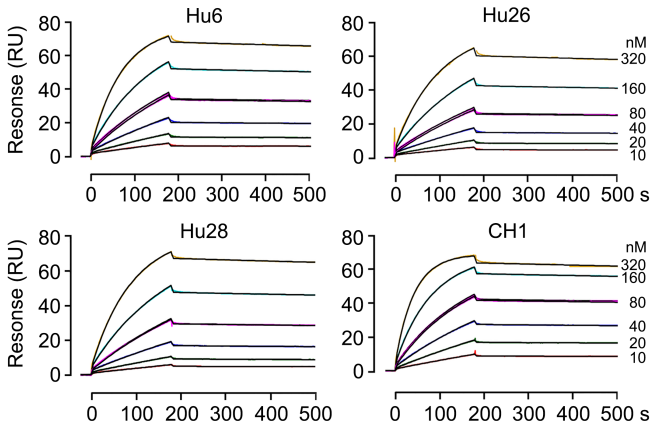

Extended Data Figure 3: FSH–Blocking Antibodies Hu6, Hu26 and Hu28 Bind Mouse FSH. Sensograms from surface plasmon resonance measurements on Biacore 8K/T200 showing the concentration–dependent binding of humanized antibodies Hu6, Hu26 and Hu28 (10 – 320 nM) to mouse FSH. Please also refer to Fig. 1a and Table 1.

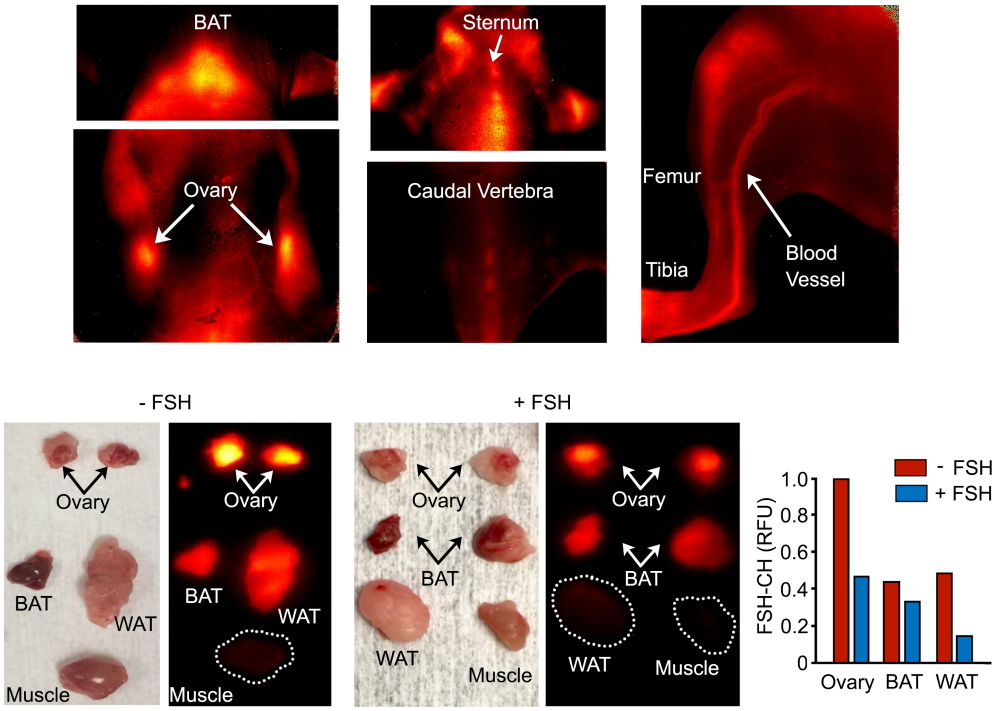

Extended Data Figure 4: FSH Binding to White and Brown Adipose Tissue. NIR-II imaging of FSHR–expressing tissues 2 hours after injection of FSH-CH (12.5 μg) into the tail vein of mice. Signal in intact (top) and dissected tissues (bottom), namely ovaries, brown adipose tissues (BAT) and white adipose tissue (WAT). Attenuation of the NIR-II signal when FSH-CH was injected with a 30–fold molar excess of unconjugated FSH (bottom). Normalized fluorescence intensity for each tissue is also shown.

Anti-FSHβ Ab	K_a ($x10^4 M^{-1}s^{-1}$)	K_d ($x10^{-4}s^{-1}$)	K_D (nM)
Hu28	1.53	1.66	10.80
Hu6	1.00	2.14	21.40
Hu26	1.71	2.52	14.70
Hu14	1.35	3.03	22.40
Hu27	0.95	3.08	32.40
Hu12	0.17	3.22	191.00
Hu22	1.62	3.32	20.50
Hu4	1.41	3.34	23.70
CH2	2.39	3.88	16.20
Hu3	0.79	4.09	51.60
Hu5	0.77	4.38	56.90
Hu25	3.51	4.43	12.60
Hu30	3.37	4.54	13.50
Hu19	2.10	4.59	21.90
Hu20	1.35	4.65	34.40
Hu8	2.02	4.69	23.30
Hu24	0.98	5.13	52.50
Hu29	3.89	5.58	14.40
Hu18	1.57	5.62	35.80
Hu11	2.21	5.66	25.60
Hu16	1.66	5.71	34.30
Hu21	1.95	5.84	29.90
Hu2	2.21	5.98	27.00
Hu10	1.94	6.21	32.10
Hu13	0.05	7.76	1690.00
Hu9	3.24	8.26	25.50
Hu17	4.85	10.90	22.50
Hu1	5.29	12.00	22.70
CH1	5.54	12.70	23.00
Hu15	3.22	14.60	45.30
Hu23	3.02	21.80	72.30
Hu7	5.06	23.60	46.50

Extended Data Table 1: FSH Binding to 30 Antibody–Expressing Bacterial Lysates. Surface plasmon resonance (SPR, Biacore) utilized to study the binding properties of human FSH with the crude bacterial lysates of 30 humanized clones of the anti–FSHβ antibody Hf2[28]. These yielded measures of association constant (K_a), dissociation constant (K_d) and affinity (K_D). Clone 28, 6 and 26 displayed lowest K_d, and were thus chosen for purification and further characterization.